Electronic Supplementary Information

Role of the shape in substrate-induced plasmonic shift and mode uncovering on gold nanocrystals

Feng Qin,[a,b] Ximin Cui,[a] Qifeng Ruan,[a] Yunhe Lai,[a] Jianfang Wang,*[a] Hongge Ma[b] and Hai-Qing Lin[c]

a Department of Physics, The Chinese University of Hong Kong, Shatin, Hong Kong SAR, China. E-mail: jfwang@phy.cuhk.edu.hk

b Science and Technology on High Power Microwave Laboratory, Institute of Applied Electronics, China Academy of Engineering Physics, Mianyang 621900, Sichuan Province, China

c Beijing Computational Science Research Center, Beijing 100193, China
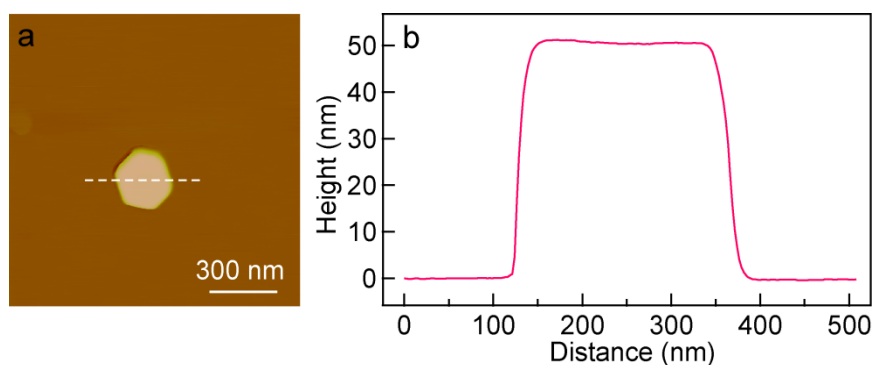
Fig. S1 AFM measurement. (a) Height image of a single NPL from AuNPL7. (b) Height profile that is extracted along the white dashed line indicated in (a).
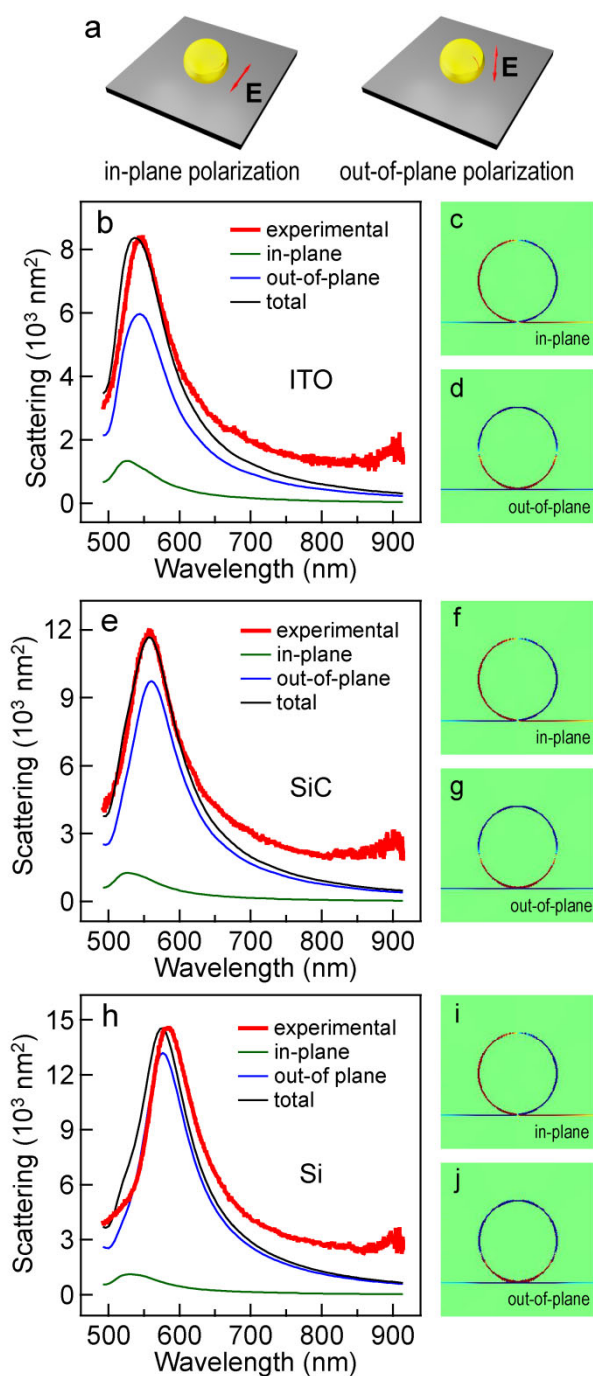
Fig. S2 FDTD simulations of the Au NSs. (a) Schematics showing the different excitation configurations. The red arrow indicates the direction of the excitation electric field. On the left is the in-plane-polarized excitation, where the electric field is parallel to the substrate. On the right is the out-of-plane-polarized excitation, where the electric field is perpendicular to the substrate. (b) Experimental (red) and simulated scattering spectra of an individual NS supported on the ITO substrate. (c,d) Charge distribution contours at the plasmon peak wavelengths for the in-plane and out-of-plane excitations. The red and blue colors represent positive and negative charges, respectively. (e–j) Corresponding simulation results for an

individual NS supported on the SiC substrate and Si substrate, respectively. In order to facilitate the comparison between the measured and simulated scattering spectra, care were taken in plotting the experimental spectra in (b, e and h) with respect to the right axis. First, the scale of the right axis is linear. Second, the zero point of the right axis is fixed at the same height as that of the left axis. Third, the range of the right axis is carefully adjusted to make the peak of the experimental spectrum nearly at the same height as that of the total simulated scattering spectrum. The green and blue curves in (b, e and h) represent the scattering spectra simulated under the in-plane and out-of-plane excitations, respectively. The total scattering spectrum (black) is obtained by adding together the blue spectrum and twice the green spectrum.
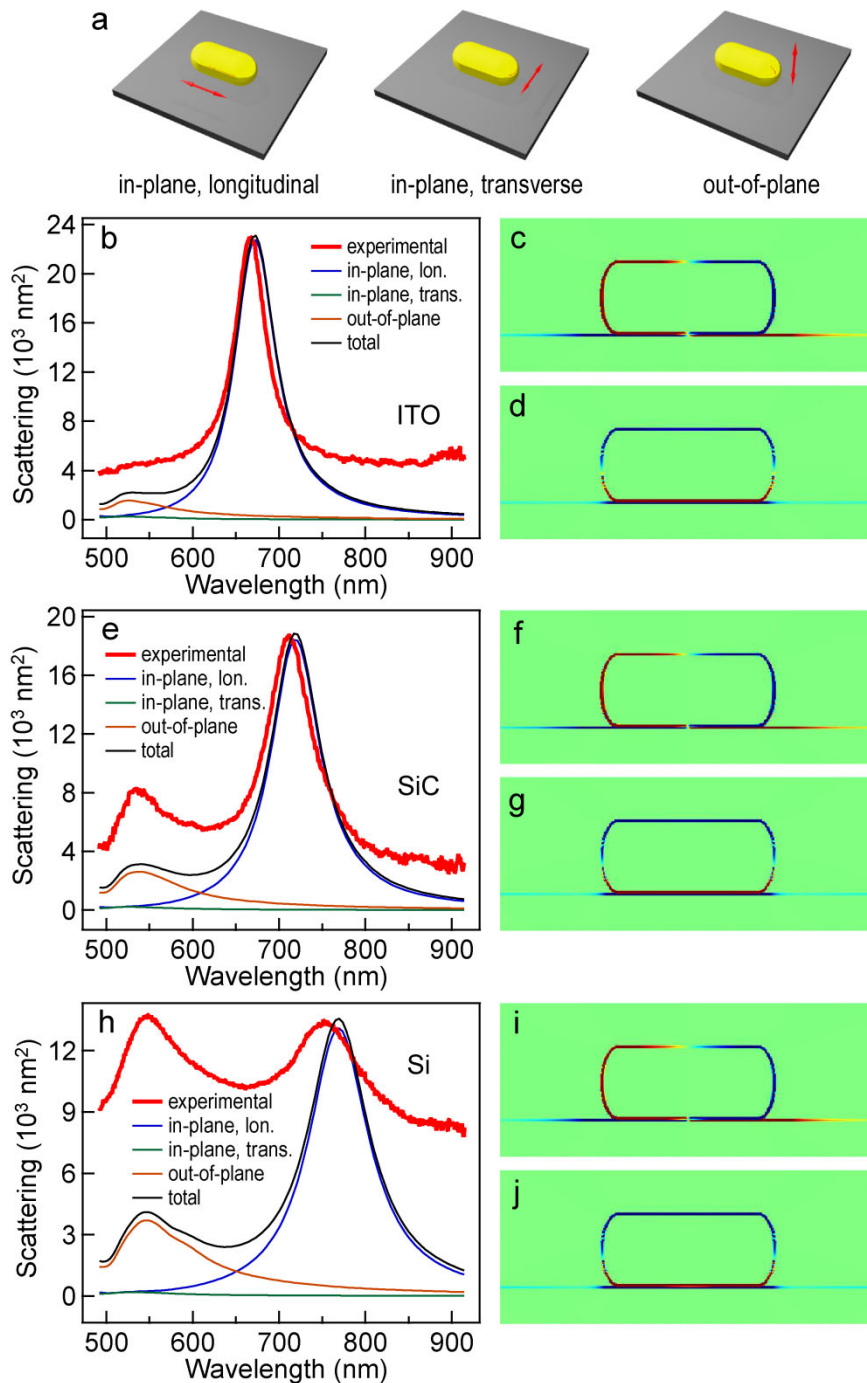
Fig. S3 FDTD simulation results of the Au NRs. (a) Schematics showing the three different excitation configurations. The red arrow indicates the direction of the excitation electric field. The NR lies parallel to the substrate. At the left, the excitation electric field is parallel to the length axis of the nanorod. In the middle, the electric field is perpendicular to the length axis of the nanorod and parallel to the substrate. At the right, the electric field is perpendicular to the substrate plane. The three configurations are called the in-plane longitudinal, in-plane transverse and out-of-plane excitations, respectively. (b) Experimental (red) and simulated scattering spectra of an individual Au NR supported on the ITO

substrate. (c,d) Charge distribution contours at the plasmon peak wavelengths for the in-plane longitudinal and out-of-plane excitations. (e–j) Corresponding results for an individual Au NR supported on SiC and Si, respectively. The measured spectra have been adjusted as described above to facilitate the comparison between the experiments and simulations. The blue, green and orange curves represent the spectra simulated under the in-plane longitudinal, in-plane transverse and out-of-plane excitations, respectively. The total spectrum (black) is the sum of the three curves. The charge distribution contours of the in-plane transverse plasmon mode are not given because the plasmon mode is too weak. There exists a spectral discrepancy between the experiments and simulations, especially on Si, as shown in (h), where the higher-energy peak is much stronger in the experiments than in the simulations. This discrepancy is mainly caused by the fractional surface area of the NR that is in direct contact with the supporting substrate. In the simulations, the NR was modeled as a nanocylinder capped with a half ellipsoid at each end. A perfect line contact with the substrate is assumed for the NR, leading to a fractional contact area of 0%. In contrast, the NRs used in our study are faceted. Their fractional contact area was determined to be 18%. Such a finite fractional contact area intensifies the out-of-plane plasmon mode of the NR supported on the different substrates in the experiments.
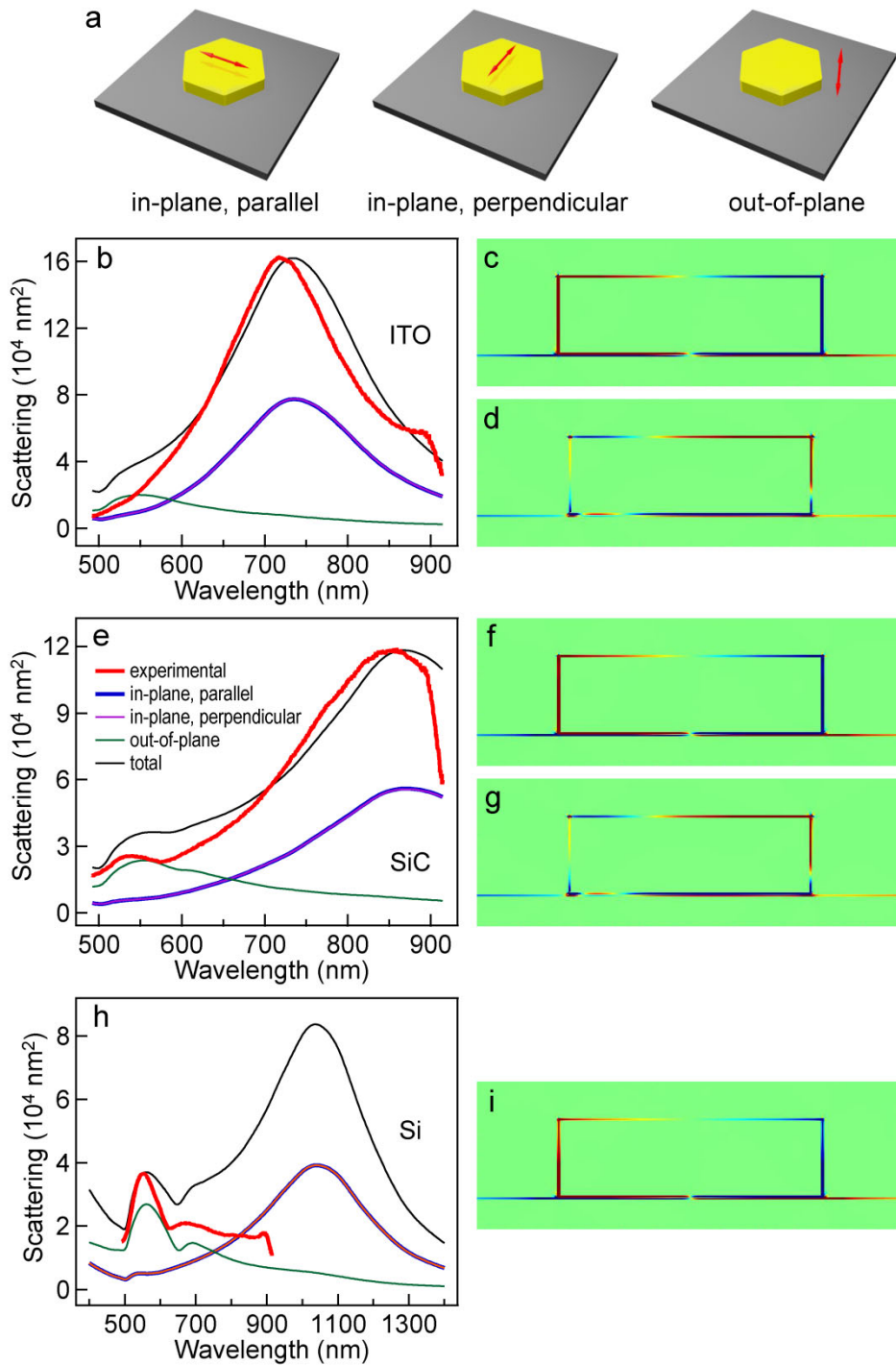
Fig. S4 FDTD simulation results of the Au NPLs from the AuNPL7 sample. (a) Schematics showing the three different excitation configurations. The red arrow indicates the direction of the excitation electric field. The NPL lies parallel to the substrate. At the left, the electric field of the excitation light is parallel to the substrate plane and also parallel to one pair of opposite edges of the NPL. In the middle, the electric field is parallel to the substrate plane and perpendicular to one pair of opposite edges of the NPL. At the right, the electric field is perpendicular to the substrate plane. (b) Experimental (red) and simulated scattering

spectra of an individual Au NPL supported on the ITO substrate. (c,d) Charge distribution contours simulated at the peak wavelengths under the in-plane parallel and out-of-plane excitations. (e) Experimental (red) and simulated scattering spectra of an individual Au NPL supported on the SiC substrate. (f,g) Charge distribution contours simulated at the peak wavelengths under the in-plane parallel and out-of-plane excitations. (h) Experimental (red) and simulated scattering spectra of an individual Au NPL supported on the Si substrate. (i) Charge distribution contour simulated at the peak wavelength under the in-plane parallel excitation. The experimental spectra have been adjusted as described above to facilitate the comparison between the experiments and simulations. The blue and purple spectra were simulated under the in-plane parallel and in-plane perpendicular excitations, respectively. The two spectra on each substrate overlap well with each other owing to the symmetry of the hexagonal NPL. The green spectra were simulated under the out-of-plane excitation. The total spectra (black) are the sum of the three spectra simulated under the different excitation configurations.
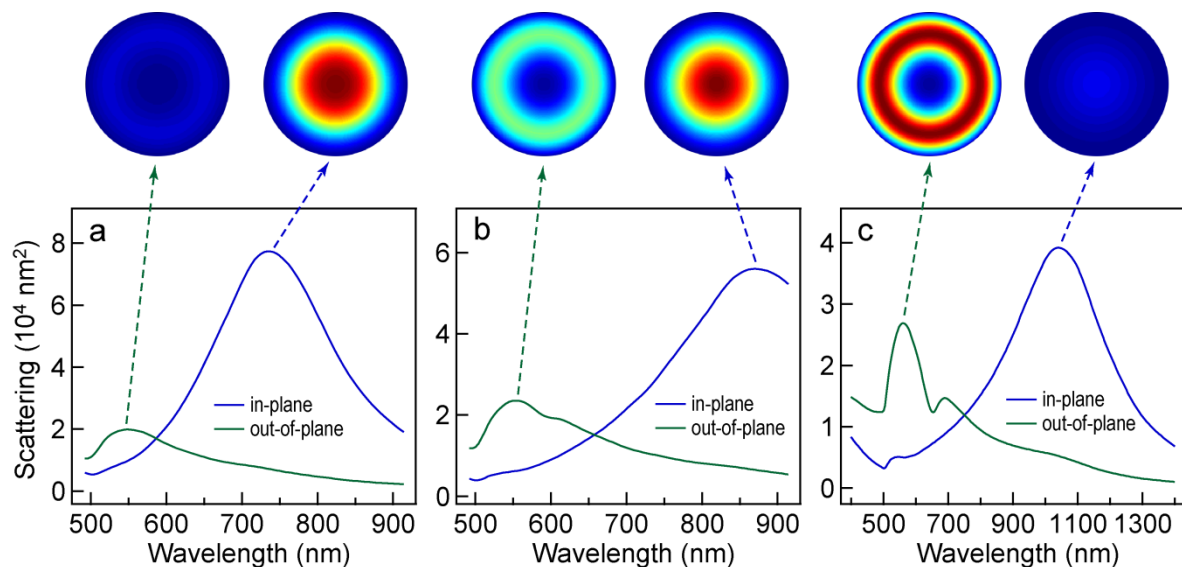
Fig. S5 FDTD-simulated scattering spectra and far-field scattering patterns of the NPLs from the AuNPL7 sample supported on ITO, SiC and Si. (a) On ITO. (b) On SiC. (c) On Si. During the simulation of the scattering patterns, the wavelength-dependent responsivity of the camera is not taken into account. On ITO and SiC, the scattering intensity of the in-plane plasmon mode is larger than that of the out-of-plane one. In contrast, on Si, the scattering intensity of the out-of-plane plasmon mode is larger than that of the in-plane one. The intensity reversal is due to the difference in the energy flow behavior. The energy flowing towards

the air side, which is opposite to the substrate side, for the in-plane and out-of-plane modes are 3.9% and 28.6%, respectively.
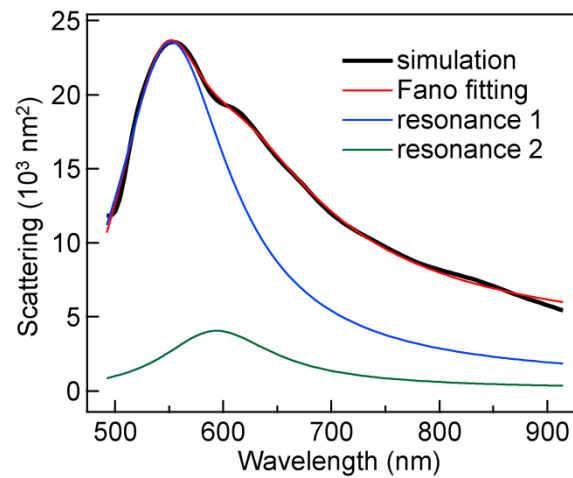
Fig. S6 Fitting of the FDTD-simulated scattering spectrum of a Au NPL from AuNPL7. The NPL is supported on the SiC substrate. The fitting is based on the Fano interference model. The parameters resulting from the fitting are a = −0.153, b_1 = 1.045, E_1 = 2.233 eV, Γ_1 = 0.291 eV, φ_1 = 1.89π, b_2 = 0.415, E_2 = 2.09 eV, Γ_2 = 0.185 eV, φ_2 = 0.0519π. The scattering spectrum (black) was simulated under the out-of-plane excitation. The red curve is the Fano fitting. The blue and green curves are the contributions from the two resonances.
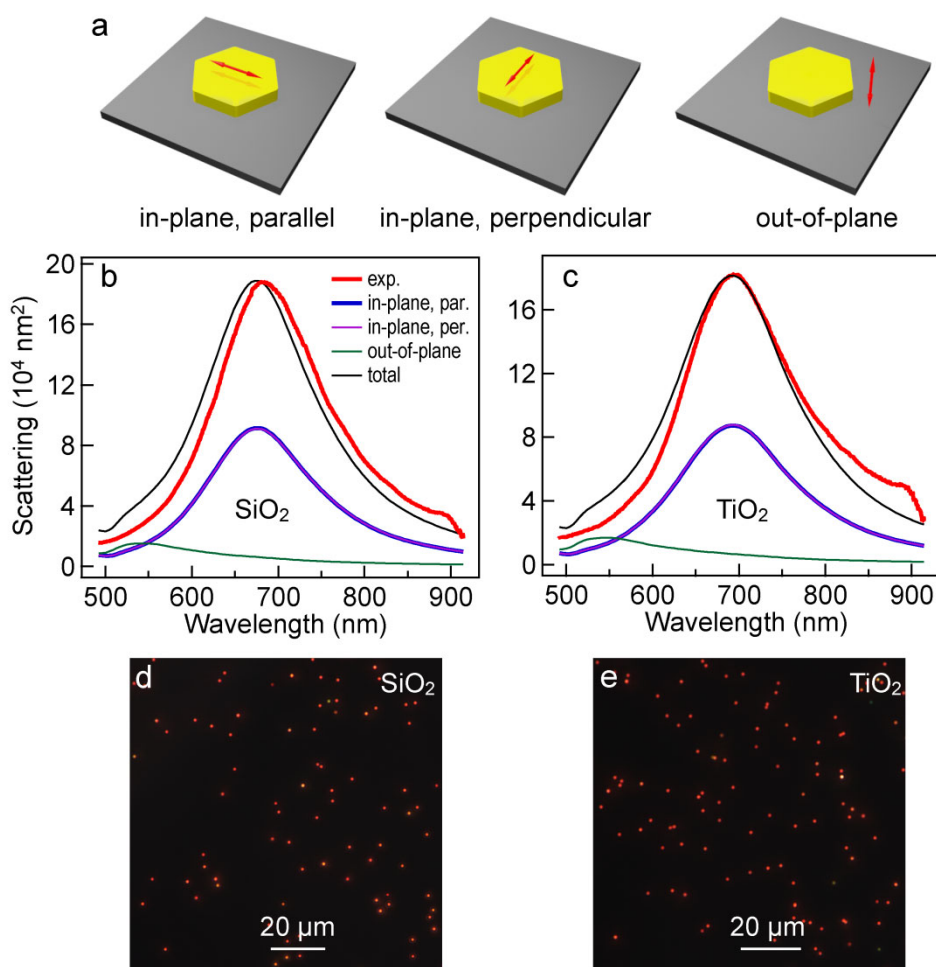
Fig. S7 Scattering spectra and far-field scattering images of the spatially isolated NPLs from the AuNPL7 sample. The sample is deposited on glass slides or mesostructured TiO$_2$ films. (a) Schematics showing the three different excitation configurations. (b,c) Experimental (red) and simulated scattering spectra of the Au NPL supported on a glass slide and mesostructured TiO$_2$ film, respectively. The blue and purple curves were obtained from the simulations under the in-plane parallel and in-plane perpendicular excitations. The green curve was obtained from the simulation under the out-of-plane excitation. The black curve represents the sum of the three curves. (d,e) Far-field scattering images of the Au NPLs deposited on a glass slide and mesostructured TiO$_2$ film, respectively.
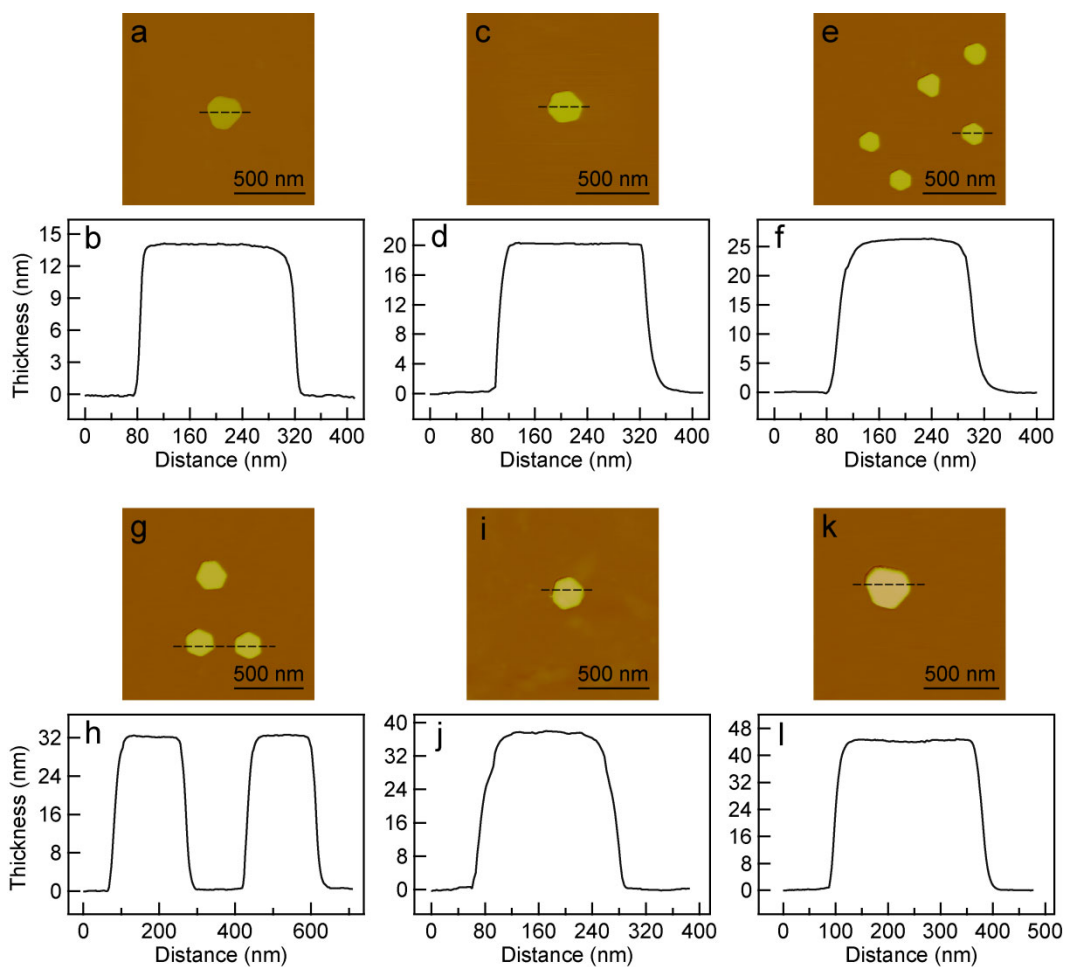
Fig. S8 Representative AFM images of AuNPL1–6 and the corresponding height profiles. (a,b) AuNPL1. (c,d) AuNPL2. (e,f) AuNPL3. (g,h) AuNPL4. (i,j) AuNPL5. (k,l) AuNPL6.
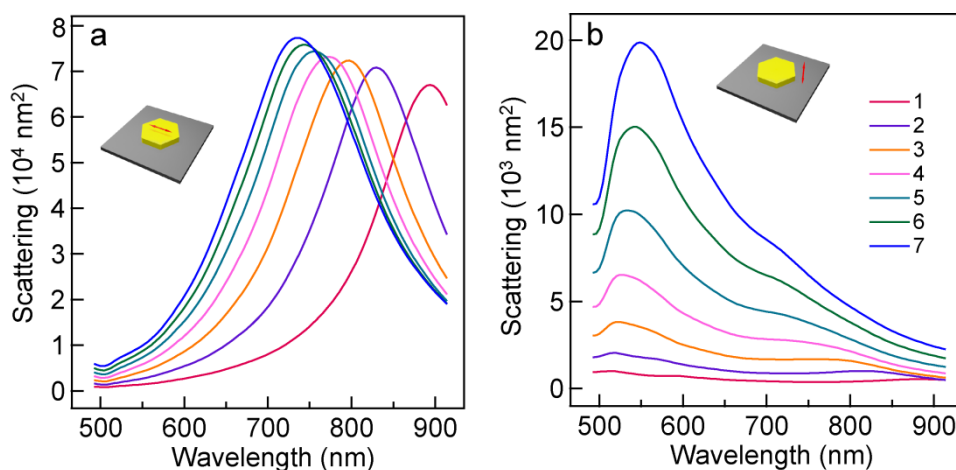
Fig. S9 Simulated scattering spectra of AuNPL1–7 supported on ITO under the different excitation polarizations. (a) In-plane parallel excitation. (b) Out-of-plane excitation. The insets are the schematics illustrating the excitation configurations. The curves labeled with 1 to 7 correspond to the simulated scattering spectra of AuNPL1–7.
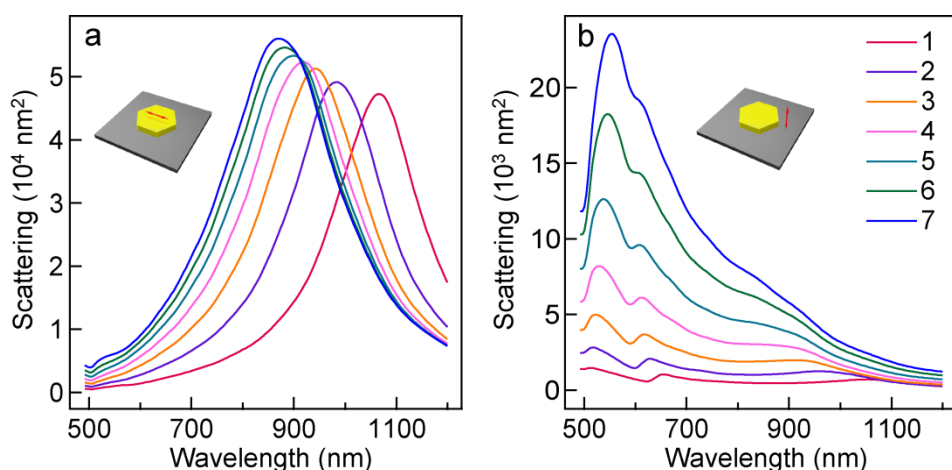
Fig. S10 Simulated scattering spectra of AuNPL1–7 supported on SiC substrates under the different excitation polarizations. (a) In-plane parallel excitation. (b) Out-of-plane excitation. The insets are the schematics illustrating the excitation configurations. The curves labeled with 1 to 7 correspond to the simulated scattering spectra of AuNPL1–7.
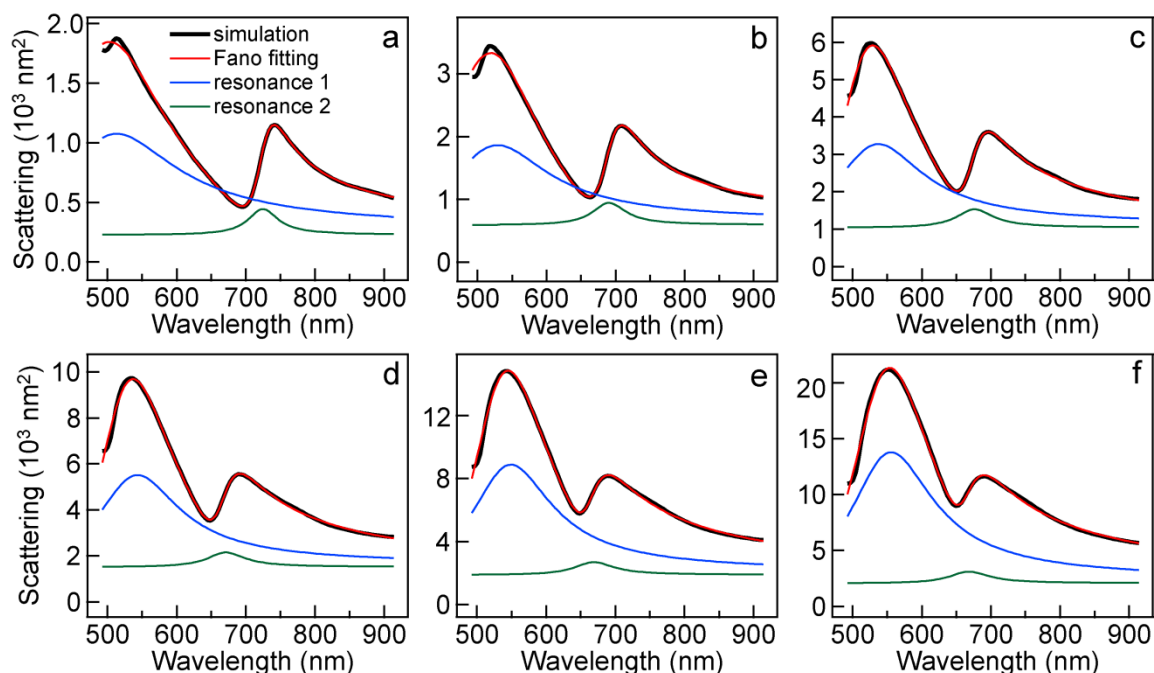
Fig. S11 Fitting of the simulated scattering spectra of AuNPL1–6 supported on Si according to the Fano interference model. (a) AuNPL1. (b) AuNPL2. (c) AuNPL3. (d) AuNPL4. (e) AuNPL5. (f) AuNPL6. The parameters obtained from the fitting are listed in Table S1†. The black and red curves represent the FDTD-simulated and Fano-fitted spectra. The blue and green curves are the separate contributions from the two resonances.

Table S1 Parameters obtained from fitting the simulated scattering spectra of AuNPL1–7 supported on Si according to the Fano interference model

Sample	a	b_1	E_1 (eV)	Γ_1 (eV)	φ_1 (π)	b_2	E_2 (eV)	Γ_2 (eV)	φ_2 (π)	b_2/b_1
AuNPL1	-0.427	0.602	2.377	0.493	0.407	0.337	1.711	0.0626	0.765	0.56
AuNPL2	-0.415	0.608	2.345	0.392	0.423	0.321	1.796	0.077	0.82	0.528
AuNPL3	-0.418	0.611	2.308	0.334	0.456	0.286	1.833	0.087	0.853	0.468
AuNPL4	-0.394	0.641	2.283	0.305	0.496	0.255	1.848	0.0922	0.891	0.398
AuNPL5	-0.357	0.687	2.259	0.293	0.538	0.234	1.853	0.0952	0.916	0.341
AuNPL6	-0.312	0.744	2.231	0.294	0.575	0.222	1.856	0.097	0.969	0.298
AuNPL7	-0.236	0.835	2.203	0.306	0.625	0.212	1.858	0.0988	0.051	0.254